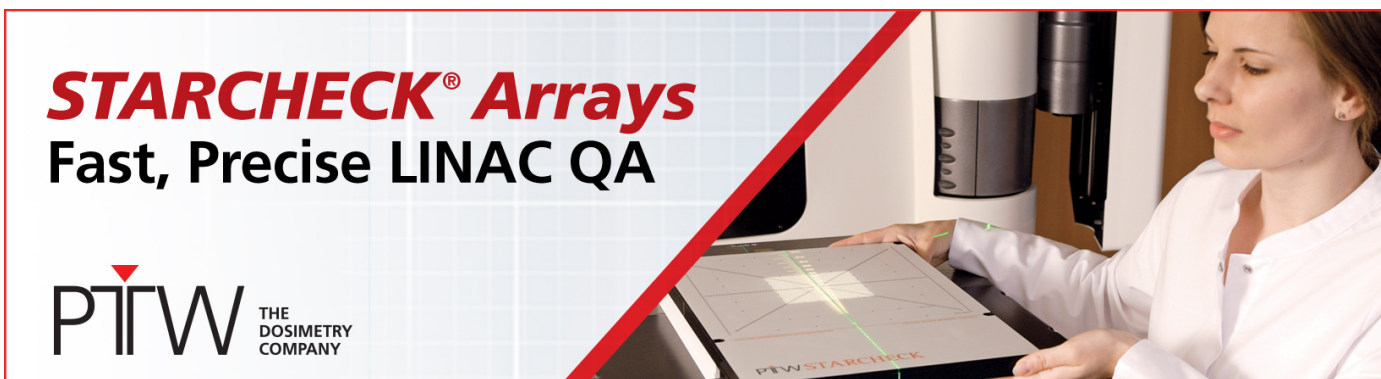


PAPER

Time-based signal sampling using sawtooth-shaped threshold

To cite this article: Guen Bae Ko and Jae Sung Lee 2019 *Phys. Med. Biol.* **64** 125020

View the [article online](#) for updates and enhancements.



STARCHECK® Arrays
Fast, Precise LINAC QA

PTW THE
DOSIMETRY
COMPANY



PAPER

Time-based signal sampling using sawtooth-shaped threshold

RECEIVED
31 December 2018REVISED
13 April 2019ACCEPTED FOR PUBLICATION
3 May 2019PUBLISHED
20 June 2019Guen Bae Ko^{1,2}  and Jae Sung Lee^{1,2,3,4,5,6} ¹ Brightonix Imaging Inc., Seoul 04782, Republic of Korea² Institute of Radiation Medicine, Medical Research Center, Seoul National University College of Medicine, Seoul 03080, Republic of Korea³ Department of Nuclear Medicine, Seoul National University College of Medicine, Seoul 03080, Republic of Korea⁴ Department of Biomedical Sciences, Seoul National University College of Medicine, Seoul 03080, Republic of Korea⁵ Interdisciplinary Program in Radiation Applied Life Science, Seoul National University College of Medicine, Seoul 03080, Republic of Korea⁶ Author to whom any correspondence should be addressed.E-mail: jaes@snu.ac.kr**Keywords:** positron emission tomography, readout electronics, silicon photomultiplier, time-based readout, time-over-threshold**Abstract**

Energy measurement of scintillation pulses by using time-over-threshold (TOT) has advantages of low readout cost, low power consumption, and less complexity compared with conventional analog-to-digital converter (ADC) approaches. Therefore, TOT is attractive in positron emission tomography (PET) systems based on silicon photomultiplier (SiPM) arrays requiring many readout channels. However, poor energy resolution and linearity of TOT leads to degradation of the overall PET detector and system performance, which is unsuitable for high-performance PET systems. To overcome these limitations, we propose a novel time-based signal-sampling method, sawtooth threshold sampling (STS), for PET scintillation detectors. This method uses a sawtooth-shaped threshold signal generated adaptively to the input scintillation pulse. Based on the time difference between the rising and falling edges of the digital pulse train generated by comparing the input scintillation pulse to the sawtooth signal, we can estimate the input scintillation pulse amplitude at the several time points. We compared several curve-fitting and numerical integration methods for energy estimation from the STS samples. Coincidence data between two identical scintillation detectors composed of one-to-one coupled SiPM and LGSO crystal ($3 \times 3 \times 20 \text{ mm}^3$) was measured using the proposed STS circuit. For timing- and energy-resolution measurement, STS ($10.5\% \pm 0.21\%$ and $200 \pm 5.8 \text{ ps}$) was superior than simple TOT ($16.4\% \pm 0.52\%$ and $224 \pm 8.2 \text{ ps}$) and was similar to high-speed ADC ($9.84\% \pm 0.11\%$ and $193 \pm 4.3 \text{ ps}$). In conclusion, the proposed method can be a cost-effective solution for data collection in future SiPM-based PET systems.

Introduction

Silicon photomultipliers (SiPMs) are now widely used in scintillation detectors and replace photomultiplier tubes (PMTs) in state-of-art positron emission tomography (PET) systems. Fast response time, magnetic field insensitivity, and compact size of SiPM allow the simultaneous PET scan with magnetic resonance imaging (Yoon *et al* 2012, Grant *et al* 2016, Ko *et al* 2016a, 2016b, Schug *et al* 2016, Stortz *et al* 2017, Omidvari *et al* 2017) and lead to superior energy and timing resolutions of PET systems through improved photon-counting statistics (Schaart *et al* 2010, Kang *et al* 2015, Nemallapudi *et al* 2015, Cates and Levin 2016, Kwon *et al* 2016, Ko and Lee 2017).

However, high dark count rate and large terminal capacitance of SiPM result in the degradation of PET detector performance when output signals from multiple SiPMs are combined to configure sufficiently large area detectors for PET imaging (Lee and Hong 2010, Kwon and Lee 2014). To reduce such performance degradation, multiplexing methods that reduce the effective capacitance through capacitive coupling rather than resistive coupling were suggested (Bieniosek *et al* 2016, Park *et al* 2017). Nonetheless, the timing performance of these

multiplexing methods is still limited by the accumulation of dark current. Therefore, reducing the multiplexed detector area and applying individual signal readout from SiPM is preferred in the time-of-flight (TOF) PET detectors; however, these approaches require a large number of readout channels.

Accordingly, the digitization of a large number of signals sent from SiPM-based PET detectors without degradation of their physical characteristics such as energy, timing, and spatial resolutions has been actively investigated. In general, the best detector performance can be achieved using high-speed free-running analog-to-digital converters (ADCs) (Schaart *et al* 2010, Yeom *et al* 2013, Cates and Levin 2016).

However, free-running ADCs are expensive and consume significant power. A less expensive solution, both in cost and power, is the time-over-threshold (TOT) method, which uses a comparator with constant threshold voltage to convert pulse height to temporal width proportional to energy (Powolny *et al* 2008, 2011, Won *et al* 2016a). The temporal width is then measured using a time-to-digital converter (TDC) or counter circuit. Therefore, we call this type of method time-based readout. TOT is a simple and cost-effective method that might be suitable for highly dense radiation counting systems. However, the pulse-shape information is lost in the TOT, which is necessary for distinguishing the scintillation crystals from a phoswich PET detectors. The phoswich detector enables the depth-of-interaction (DOI) measurement (Seidel *et al* 1999, Ito *et al* 2011) or improves the spatial resolution (Bergeron *et al* 2009) through the pulse-shape discrimination (PSD). Although a TOT-based DOI detection method was suggested (Chang *et al* 2017), this method requires additional pulse amplitude measurement to avoid the DOI mis-classification due to Compton scattering. Nonlinear relationship between input charge proportional to absorbed radiation energy by scintillation detector and TOT outcome is another drawback of TOT, which is accompanied with the trade-off between energy and timing resolutions and dynamic range. Accurate timing information is particularly important in TOF PET systems because better timing resolution leads to better image quality (Karp *et al* 2008, Conti 2011). Energy information should also be accurate because it helps in rejecting scattered events and recovering inter-crystal scattering events (Wagadarikar *et al* 2014, Lage *et al* 2015, Fu *et al* 2016, Lee *et al* 2018a, 2018b).

Although several different approaches have been suggested to overcome the drawbacks of TOT, they still have some limitations. One of these approaches is the pulse-width modulation (or charge-to-digital converter), which provides linearly decayed output signal by discharging constant current from the stored charge or pulse peak from the detector (Parl *et al* 2012, Bieniosek *et al* 2013). The linear decay of output signal yields better energy linearity. TOT using two different threshold voltage levels (dual-threshold TOT) also improves energy linearity (Grant and Levin 2014, Ko and Lee 2017). Reducing the trade-off between energy and timing resolutions is another advantage of the dual-threshold TOT. Dynamic TOT method, in which the dynamically varying threshold is applied following pulse shaping, improves energy linearity and dynamic range at the expense of timing performance degradation due to pulse shaping. In the dynamic TOT method, linearity between energy and TOT can be achieved by selecting a threshold function depending on the input signal shape (Shimazoe *et al* 2012, Yonggang *et al* 2014). Although abovementioned variations of TOT have overcome many limitations of the original TOT, they still have some disadvantages in different aspects such as poor timing performance. In addition, decay time information on the scintillation pulse, which enables DOI measurement, is not provided by the abovementioned TOT variations. Scintillation pulse shape can be reconstructed by applying multi-voltage thresholds (MVTs) (Xie *et al* 2005, Kim *et al* 2009, Xi *et al* 2013). However, the MVT method requires multiple comparators and digital readout channels, which weakens the best advantage of TOT, simplicity.

Here, we propose a novel time-based signal sampling method for scintillation detectors. In the proposed method, a sawtooth-shaped threshold signal is generated adaptively to the input pulse for generating output digital pulses. Then, the input signal is restored by applying curve-fitting or numerical integration methods. We compared the timing and energy performance of the proposed method with those of digitization methods using high-speed free-running ADC and TOT. The PSD for two different scintillation crystals with different decay times using the proposed method were also demonstrated. The main advantage of the proposed method over MVT is that it needs only single comparator and digital readout channel.

Methods

Concept of sawtooth threshold sampling

The output pulse from the scintillation detectors used in TOF PET rapidly increases from the baseline and slowly decays exponentially. The rising edge of the scintillation pulse possesses information on the photon arrival time. The peak amplitude and area (i.e. charge) of scintillation pulse is proportional to the absorbed gamma-ray energy by the detector. In phoswich-type detectors (Dahlbom *et al* 1997, Seidel *et al* 1999, Hong *et al* 2008), the pulse shape characterized by the decay time provides DOI information. Typically, the scintillation pulse can be represented by a biexponential model as follows:

$$S(t) = \begin{cases} 0 & \text{if } t < t_0 \\ ae^{-(t-t_0)/\tau_d}(1 - e^{-(t-t_0)/\tau_r}) & \text{if } t \geq t_0 \end{cases}, \quad (1)$$

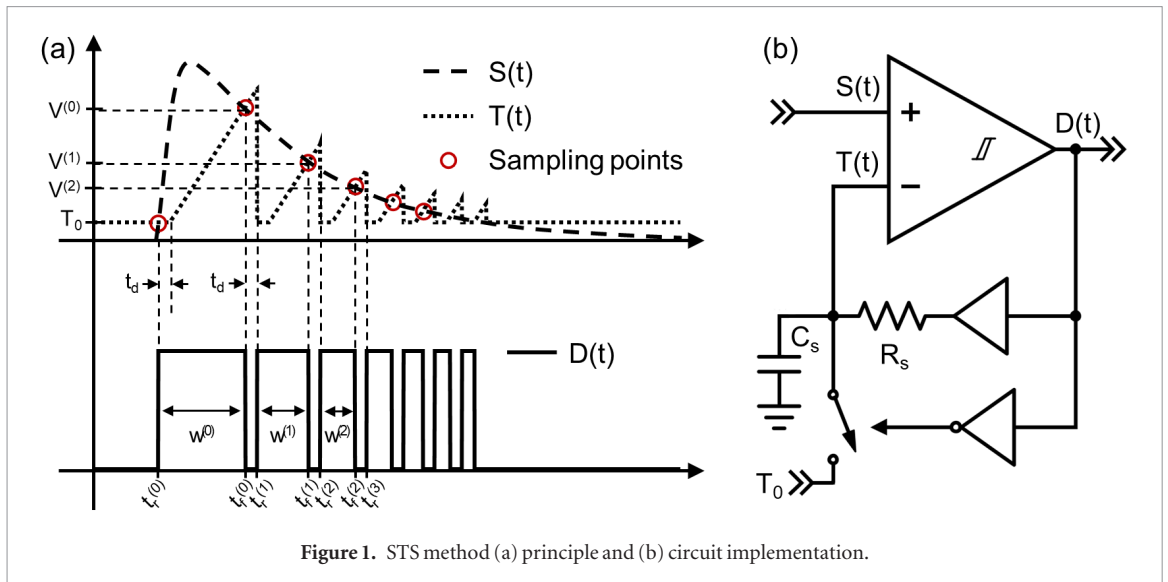


Figure 1. STS method (a) principle and (b) circuit implementation.

where t_0 is pulse onset time, a is amplitude, τ_d is decay time, and τ_r is rise time parameter. The biexponential model accurately describes the shape of the scintillation pulse, allowing the accurate prediction of timing resolution (Shao 2007).

Equation (1) shows that noiseless scintillation pulse shape can be estimated from only four data samples. Much smaller number of sampling points than that provided by high-speed free-running ADC might be necessary for pulse-shape estimation based on the biexponential modeling.

Sawtooth threshold sampling (STS) method proposed in this paper is based on the biexponential modeling of scintillation pulse. In this method, output digital pulse train (solid line in figure 1(a)) is generated by comparing the input scintillation pulse (dashed line in figure 1(a)) and adaptively generated sawtooth-shaped threshold (dotted line in figure 1(a)). The voltage level of sampling points on the input pulse can be estimated from the width of squares of output signal and the slope of sawtooth signal. Many data samples (red circles in figure 1(a)) obtained, as shown in figure 1(a), enables us to retrieve energy and time information from digital output.

This STS circuit can be simply implemented using some basic circuit components including comparator, buffer, inverter, analog switch, resistor, and capacitor (figure 1(b)). The initial threshold, T_0 should be set to avoid false triggering due to electrical noise. This circuit operates in the following way: (1) When the input pulse [$S(t)$] is smaller than the initial threshold voltage, the threshold voltage [$T(t)$] is T_0 because the comparator output [$D(t)$] is low, and thus the analog switch remains closed. (2) When the input signal reaches T_0 , the comparator output goes to high and then the analog switch opens. (3) Threshold voltage ramps up from T_0 with RC time constant ($R_s C_s$) until it crosses the input pulse. (4) When the threshold voltage becomes larger than the input pulse, the comparator output goes to low, analog switch is closed, and threshold voltage quickly falls to initial threshold. (5) These operations are repeated until the input pulse is decayed below initial threshold.

The change in threshold voltage over time can be expressed by the following equation, considering the propagation delay of circuit components and printed circuit board trace.

$$T(t) = \begin{cases} T_0 & \text{if } t < t_r^{(0)}, t_r^{(i)} \leq t < t_r^{(i)} + t_d \\ (V_{OH} - T_0)(1 - e^{-\frac{t - (t_r^{(i)} + t_d)}{R_s C_s}}) + T_0 & \\ \text{if } t_r^{(i)} + t_d \leq t < t_f^{(i)} + t_d & \end{cases}, \quad (2)$$

where V_{OH} is the high-level output voltage of the buffer, R_s and C_s are the resistance and capacitance, respectively, of the low-pass filter for sawtooth slope generation, t_d is the propagation delay from the comparator input to buffer output, $t_r^{(i)}$ is the occurrence time of i th rising edge in the output pulse train, and $t_f^{(i)}$ is the occurrence time of i th falling edge in the output pulse train. Because $t_f^{(i)}$ is the time when $S(t)$ and $T(t)$ are equal, the voltage level at each sampling point can be calculated using only the time information offered by the output pulse train ($t_r^{(i)}$, $t_f^{(i)}$, and $W^{(i)} = t_f^{(i)} - t_r^{(i)}$) as follows:

$$V(t_r^{(0)}) = T_0 \quad (3)$$

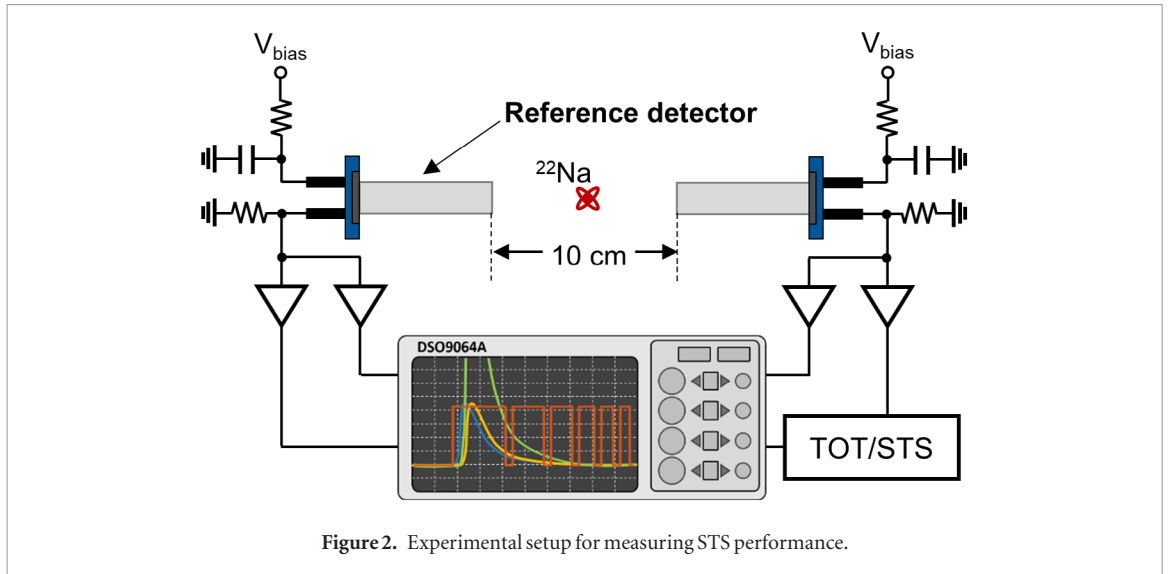


Figure 2. Experimental setup for measuring STS performance.

$$\begin{aligned}
 V(t_f^{(i)}) &= T(t_f^{(i)}) \\
 &= (V_{OH} - T_0) \left(1 - e^{-\frac{t_f^{(i)} - (t_f^{(i)} + t_d)}{R_S C_S}}\right) + T_0 \\
 &= (V_{OH} - T_0) \left(1 - e^{-\frac{W^{(i)} - t_d}{R_S C_S}}\right) + T_0 \\
 &= V_{OH} - (V_{OH} - T_0) e^{\frac{t_d}{R_S C_S}} e^{-\frac{W^{(i)}}{R_S C_S}}.
 \end{aligned} \tag{4}$$

If $W^{(i)} \ll R_S C_S$, equation (4) can be linearly approximated as in equation (5).

$$\begin{aligned}
 V(t_f^{(i)}) &= V_{OH} + (V_{OH} - T_0) \frac{e^{\frac{t_d}{R_S C_S}}}{R_S C_S} W^{(i)} \\
 &= P_1 + P_2 W^{(i)}.
 \end{aligned} \tag{5}$$

Finally, the energy of the recorded scintillation events can be calculated as described in the next sections.

Experimental setup

To show the feasibility of the proposed method, the circuit shown in figure 1(b) was implemented using discrete circuit components. R_S , C_S , and T_0 were set to 30 k Ω , 15 pF, and 10 mV, respectively.

Figure 2 shows an experimental setup to evaluate the performance of the proposed method. Two identical one-to-one coupled detectors were constructed for coincidence data acquisition. Chemically polished LGSO ($\text{Lu}_{1.9}\text{Gd}_{0.1}\text{SiO}_4\text{:Ce}$; Hitachi Chemicals, Japan) crystals with $3 \times 3 \times 20 \text{ mm}^3$ dimension were used in this study. Five sides of the crystals were wrapped with enhanced specular reflectors (ESR; 3M, USA) except for one light exit surface. The crystals were optically coupled with Fondazione Bruno Kessler (FBK) near-ultraviolet high-density (NUV-HD) SiPMs with $4 \times 4 \text{ mm}^2$ active area and 30 μm microcells (Piemonte *et al* 2016).

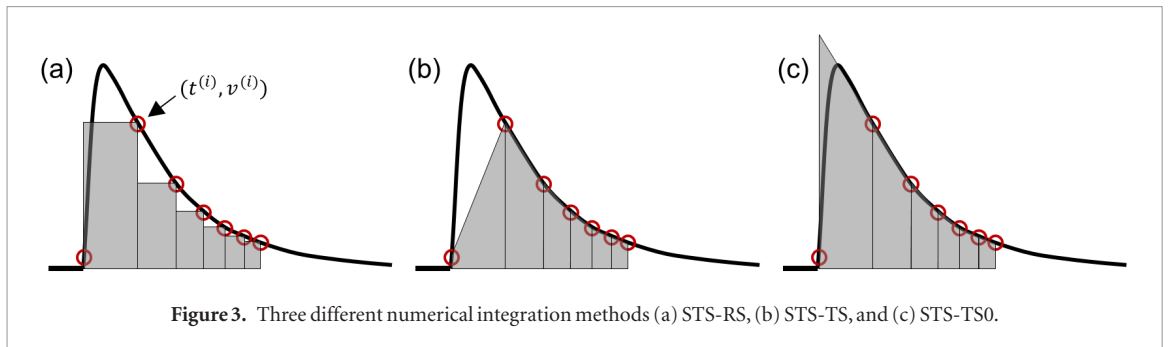
The anode signals of SiPMs were split to two amplifiers for energy and time measurement. The energy and time channels of one detector (reference detector) and energy channel of the other detector (target detector) were directly digitized using a digital oscilloscope (DSO9064A, 5 GS s^{-1} sampling speed, 600 MHz analog bandwidth, 8-bit amplitude resolution; Keysight Technologies, USA). The time channel of target detector was passed to the STS circuit. The energy channel of the target detector was used as a reference for assessing and calibrating the linearity of STS. The amplification gain of the energy signal and STS/TOT input signal was five times, but the amplification gain of the time signal connected to the oscilloscope was ten times.

The detectors were irradiated using a 23.4 μCi ^{22}Na point source located 5 cm from the detector surfaces. Both SiPMs were operated at 8.0 V above their breakdown voltage at 20 $^\circ\text{C}$. Data was repeatedly acquired five times for each experimental setup, and each data set included 20 000 coincidence events.

Width to height conversion

To acquire the time and voltage of the sampling point from the digital pulse train of the STS circuit, the pulse width [$W^{(i)}$] should be converted to the amplitude (i.e. height) of scintillation pulse using the relation in equations (4) or (5). For the first pulse of STS output, equation (5) can be expressed as follows:

$$V(t_f^{(0)}) = P_1 + P_2 W^{(0)}. \tag{6}$$



To obtain P1 and P2, 5000 data points of the width of the first pulse of the STS output pulse train $[W(0)]$ and the height of the scintillation pulse at the first falling edge $[V(t_f^{(0)})]$ were sampled from the digitalized STS signal and the scintillation signal. The P1 and P2 in equation (6) were then estimated by applying linear regression to the sampled data. Using this linear model, the sampling points on the scintillation signal could be determined from the STS pulse signal.

Energy estimation

From the sampling points derived from the STS pulse, we can estimate energy information using the following methods. In these methods, only the first six sampling points were used for pulse reconstruction.

Nonlinear least squares (STS-NLS)

The NLS method is the most common way to fit a set of data points. NLS curve fitting was applied to equation (1). For simplicity, we regarded t_0 as the point of the first rising edge of the digital pulse train ($t_r^{(0)}$). This method includes a time-consuming iterative calculation process, but it has the advantage of recovering all information, including decay time of scintillation crystal. The energy was calculated by integrating the fitted model in the 300 ns interval from the beginning of the pulse.

Linear least squares (STS-LLS)

If we know the decay and rise time of scintillation detector, τ_d and τ_r in equation (1) can be treated as constants. Therefore, equation (1) can be rewritten as the following linear equation:

$$S(t) = \begin{cases} 0 & \text{if } t < t_0 \\ ae^{-(t-t_0)/\tau_{d0}}(1 - e^{-(t-t_0)/\tau_{r0}}) & \text{if } t \geq t_0 \end{cases} \quad (7)$$

$$= \begin{cases} 0 & \text{if } t < t_0 \\ af(t) & \text{if } t \geq t_0 \end{cases},$$

where τ_{d0} and τ_{r0} are constant decay time and rise time, respectively.

Thus, using the linear model described in equation (7), the fitting can be simplified, from nonlinear to linear. Compared with the STS-NLS method, the STS-LLS method includes an analytical computation process with a simple matrix operation and is more robust to noise because fewer variables are to be estimated. τ_{d0} and τ_{r0} were determined by averaging 1000 digitized waveforms and fitting them to a biexponential model. The energy information was simply determined by fitting parameter a because the integration of fitted model is proportional to a .

Rectangular sum (STS-RS)

A basic way to obtain energy information from the STS signal is numerical integration. Figure 3(a) shows the numerical integration using the rectangular rule. For n sampling points, the energy estimator of rectangular sum is expressed as follows:

$$e = \sum_{i=0}^n v^{(i+1)}(t^{(i+1)} - t^{(i)}), \quad (8)$$

where $v^{(i)}$ and $t^{(i)}$ are the voltage and time of the i th sampling points, respectively.

Trapezoidal sum (STS-TS)

We also calculated energy information using numerical integration in a trapezoidal manner (figure 3(b)). For n sampling points, the energy estimator of trapezoidal sum is expressed as follows:

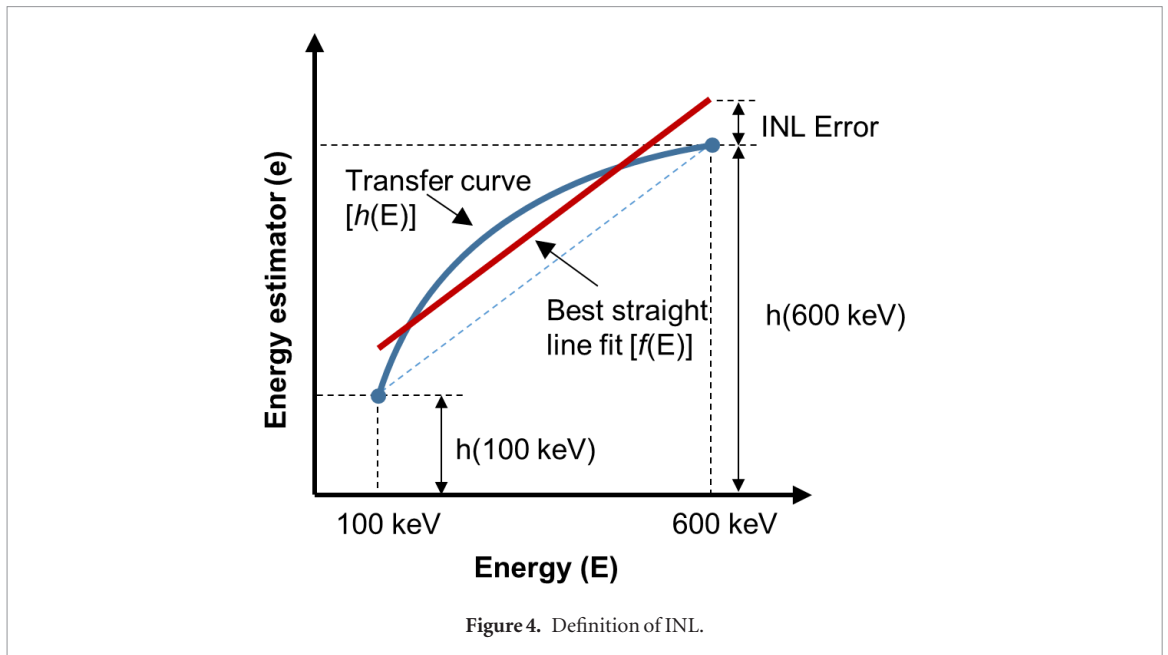


Figure 4. Definition of INL.

$$e = \sum_{i=0}^n \frac{1}{2} (v^{(i+1)} + v^{(i)}) (t^{(i+1)} - t^{(i)}). \quad (9)$$

Trapezoidal sum with zero rise time (STS-TS0)

Because the rise time of the scintillation signal is short, the simple trapezoidal sum can produce errors. To reduce this error, the STS-TS method was slightly modified, as shown in figure 3(c), and is expressed as follows:

$$e = \frac{1}{2} (2v^{(i)} - \frac{v^{(2)} - v^{(1)}}{t^{(2)} - t^{(1)}} (t^{(1)} - t^{(0)})) + \sum_{i=1}^n \frac{1}{2} (v^{(i+1)} + v^{(i)}) (t^{(i+1)} - t^{(i)}). \quad (10)$$

Energy linearity, energy resolution, and timing resolution

Energy linearity, energy resolution, and timing resolution were measured to evaluate the performance of the STS circuit.

To evaluate linearity and to apply energy calibration, the energy estimated from the proposed methods were compared with the energy obtained by the pulse integral from the oscilloscope data. We define integral nonlinearity (INL) as the figure-of-merits of energy linearity, as shown in the following equations and figure 4:

$$INL_{100-600 \text{ keV}}(E) = \frac{h(E) - f(E)}{h(600 \text{ keV}) - h(100 \text{ keV})} \quad (11)$$

$$INL_{\max} = \max[INL_{100-600 \text{ keV}}(E)] \quad (12)$$

$$INL_{\min} = \min[INL_{100-600 \text{ keV}}(E)] \quad (13)$$

$$INL_{\text{mean}} = \frac{|INL_{\max}| + |INL_{\min}|}{2}, \quad (14)$$

where energy transfer curve $h(E)$ is the energy acquired by using the proposed method as a function of real energy (calculated by pulse integral of scintillation pulse), $f(E)$ is the best-fitted straight line to $h(E)$. From the acquired data, $h(E)$ was calculated at a 20 keV interval.

For accurate energy measurement, the nonlinearity of energy estimation was calibrated using $h(E)$. Energy resolution was obtained using the corrected energy data. Coincidence timing resolution (CTR) between the target and reference detectors was measured for timing performance evaluation. The arrival time in the reference detector was extracted using a digital leading edge discriminator with a 10 mV threshold, after a baseline correction and cubic spline interpolation by a factor of 10 (Ko and Lee 2015). For the target detector, the arrival time was extracted from the first rising edge of the STS pulse train. Only the events around full-width-at-tenth-maximum from the photopeak were used for the CTR analysis.

Performance comparison with ADC and TOT

We compared the performance of the proposed method with direct waveform sampling using high-speed ADC (5 GHz sampling rate) and with TOT methods. For the ADC sampling method, the measurement setup and the analysis method for the target detector were the same as that of the reference detector. For the TOT measurement, the STS circuit was replaced by a simple comparator with a constant threshold voltage. Energy linearity, energy resolution, and CTR for TOT were measured by the same method as that in the STS data processing. To show the effect of threshold voltage on CTR, the threshold voltage of target detector was swept from 10 mV to 100 mV for all three methods, while that of the reference detector was fixed to 10 mV.

Performance dependency on sampling frequency

The accuracy of the time-based readout method is affected by the time measurement accuracy. The most preferred way to measure time is to use TDC with high precision. Implementing TDC by using the carry chain in the field programmable gate array (FPGA) can achieve a precision higher than 20 ps (Liu *et al* 2016, Won *et al* 2016b), but it uses a lot of FPGA resources. On the contrary, measuring pulse width by the number of clocks using a counter circuit requires less resources. However, the accuracy of this method is limited by the clock frequency. Therefore, to explore the effects of sampling rate of acquisition electronics on energy estimation, we implemented a virtual counter operating at 0.2, 0.1, 1.0, 2.0, and 4.0 ns clock period (i.e. 5, 2.5, 1.0, 0.5, and 0.25 GHz clock frequency, respectively) by down-sampling the measured waveform. Using the results obtained from the virtual counter, the effects of sampling rate on INL, energy resolution, and CTR for each energy estimation method were examined. In all cases, time information was recorded with a resolution of 20 ps at the first rise edge of the STS signal, under the assumption that TDC was implemented on FPGA for time measurement.

Capability of PSD

One of the advantages of the proposed method over the conventional time-based readout is the capability of PSD for DOI measurement. To prove this, two types of LGSO crystals with different levels of lutetium content, $\text{Lu}_{0.2}\text{GSO}$ ($\text{Lu}_{0.4}\text{Gd}_{1.6}\text{SiO}_4:\text{Ce}$, $\tau = 60$ ns) and $\text{Lu}_{0.95}\text{GSO}$ ($\text{Lu}_{1.9}\text{Gd}_{0.1}\text{SiO}_4:\text{Ce}$, $\tau = 40$ ns), were tested (Hong *et al* 2008, Ko *et al* 2013, Ko and Lee 2017). The size of the scintillation crystals was $1.5 \times 1.5 \times 7$ mm³ and the crystals were attached to the center of the SiPM pixel. To distinguish the scintillation crystals, pulse integrals with two different integration windows, the head integration (integration of the front part of the scintillation pulse) and the tail integration (integration of the end part of the scintillation pulse) were calculated. Using the ratio of head integration and tail integration, the pulse shape of each scintillation crystal can be distinguished (Ko and Lee 2017). The reconstructed pulse with STS-NLS method was used for the pulse integration.

Results

Reconstruction of scintillation pulse

Figure 5(a) shows the width–amplitude curve for the STS circuit with $R_S C_S = 450$ ns. The linear model in equation (6) fits well to the data because $W^{(0)} \ll R_S C_S$ was satisfied. The exponentially decaying pulse was successfully reconstructed from the STS signal using the linear relationship. The representative waveforms and reconstructed pulse by STS-NLS method are shown in figure 5(b). The reconstructed pulse was nearly identical to the original scintillation pulse.

Performance according to energy estimation method

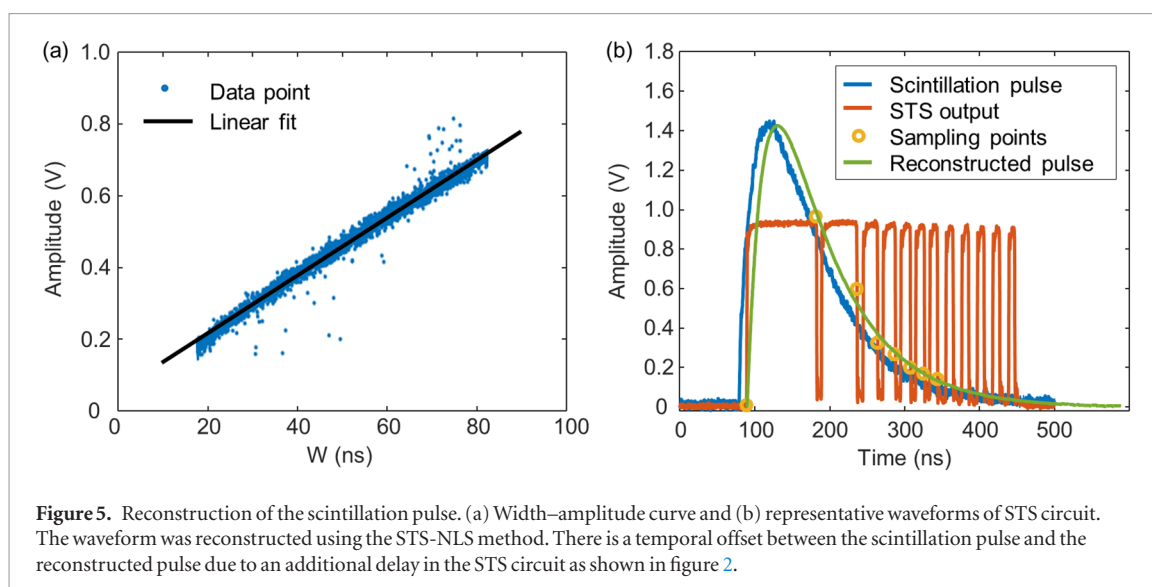
We evaluated the energy linearity of the proposed energy estimation methods for STS. Figure 6 shows the energy dependent INL for each method. Curve-fitting methods (STS-NLS and STS-LLS) generally showed better linearity than the numerical integration methods (STS-RS, STS-TS, and STS-TS0). This is mainly because numerical integration methods cannot completely estimate the area of the scintillation pulse, as shown in figure 3. Nevertheless, all STS methods showed much better linearity than the TOT method (figure 6(f)) with a threshold voltage of 100 mV.

Among the curve-fitting methods, STS-LLS performed better than STS-NLS, as predicted from a small number of estimated variables of STS-LLS. In the case of numerical integration methods, STS-TS0 showed the best performance.

The results of the quantitative evaluation are summarized in table 1. The methods with lower INL showed higher coefficient of determination, R^2 . The mean INL using STS-LLS was 0.592% and R^2 was 0.9998, which was much better than 15.4% and 0.9297 for simple TOT with 100 mV threshold.

Energy and timing resolution

Figure 7 shows the energy spectra obtained from the waveform sampling using ADC, STS-LLS, and TOT with 100 mV threshold. The energy spectra were almost identical in ADC and STS-LLS. However, the energy spectrum



obtained from TOT before linearity correction was considerably different from that obtained from the ADC because of its energy nonlinearity. Even after linearity correction, energy spectrum from TOT showed a broader photopeak than that from ADC and STS-LLS.

Figure 8 and table 2 show the energy- and timing-resolution measurement results. Energy resolution obtained using STS-LLS and that obtained by waveform sampling using ADC were not significantly different. However, energy resolution obtained from TOT was greatly degraded, especially at low threshold voltage. Although energy resolution was improved by increasing the threshold voltage, the TOT energy resolution was worse than both ADC and STS methods. Energy resolution acquired using ADC, STS-LLS, and TOT with 100 mV threshold were $9.84\% \pm 0.11\%$, $10.52\% \pm 0.21\%$, and $16.43\% \pm 0.52\%$, respectively.

The best CTR of 193.0 ± 4.3 ps was achieved using ADC with 10 mV threshold. STS-LLS with 10 mV threshold yielded 199.6 ± 5.8 ps CTR. In addition, the pattern of CTR change according to the threshold using STS was similar to that using ADC. Poor timing resolutions were acquired in TOT with low threshold because low threshold in TOT yields poor energy resolution, thus making it difficult to distinguish between photopeak and scattering events. CTR obtained using TOT with a 50 mV threshold voltage was 223.5 ps. All reported CTR values are ‘referenced’ values measured with a reference detector and ADC readout.

Table 2 indicates that all STS methods show a good detector performance although the energy resolution is slightly different depending on the energy estimation method. The pulse fitting methods (STS-NLS and STS-LLS) are generally better than the numerical integration methods (STS-RS, STS-TS, and STS-TS0) in terms of energy resolution.

Performance according to sampling frequency

Figure 9 shows the performance change of STS methods according to the sampling interval. INL was almost constant regardless of the sampling interval. The energy resolution degraded with longer sampling interval as it would cause larger quantization errors. Nevertheless, the energy resolution degradation was not significant until 1 ns sampling interval. This means that reading the STS signal using counter circuit will not degrade its performance. This is because counters operating at sampling frequencies above 1 GHz can be implemented using modern FPGAs and multiphase clocks (Yin *et al* 2012). In addition, even at a low sampling frequency of 250 MHz, the energy resolution is better than 14%, which is sufficiently good for PET systems. CTR was almost not affected by the sampling rate, indicating that the effect of degraded energy resolution with low sampling rate on scattering event rejection was not much.

DOI capability

From the reconstructed pulse using STS-NLS, the ratio of tail to head integration was calculated to distinguish two LGSO crystals. The two types of LGSO crystals are clearly different with respect to pulse-shape spectra, as shown in figure 10. Although the phoswich-type detector was not constructed, this result shows that STS would be useful for PSD.

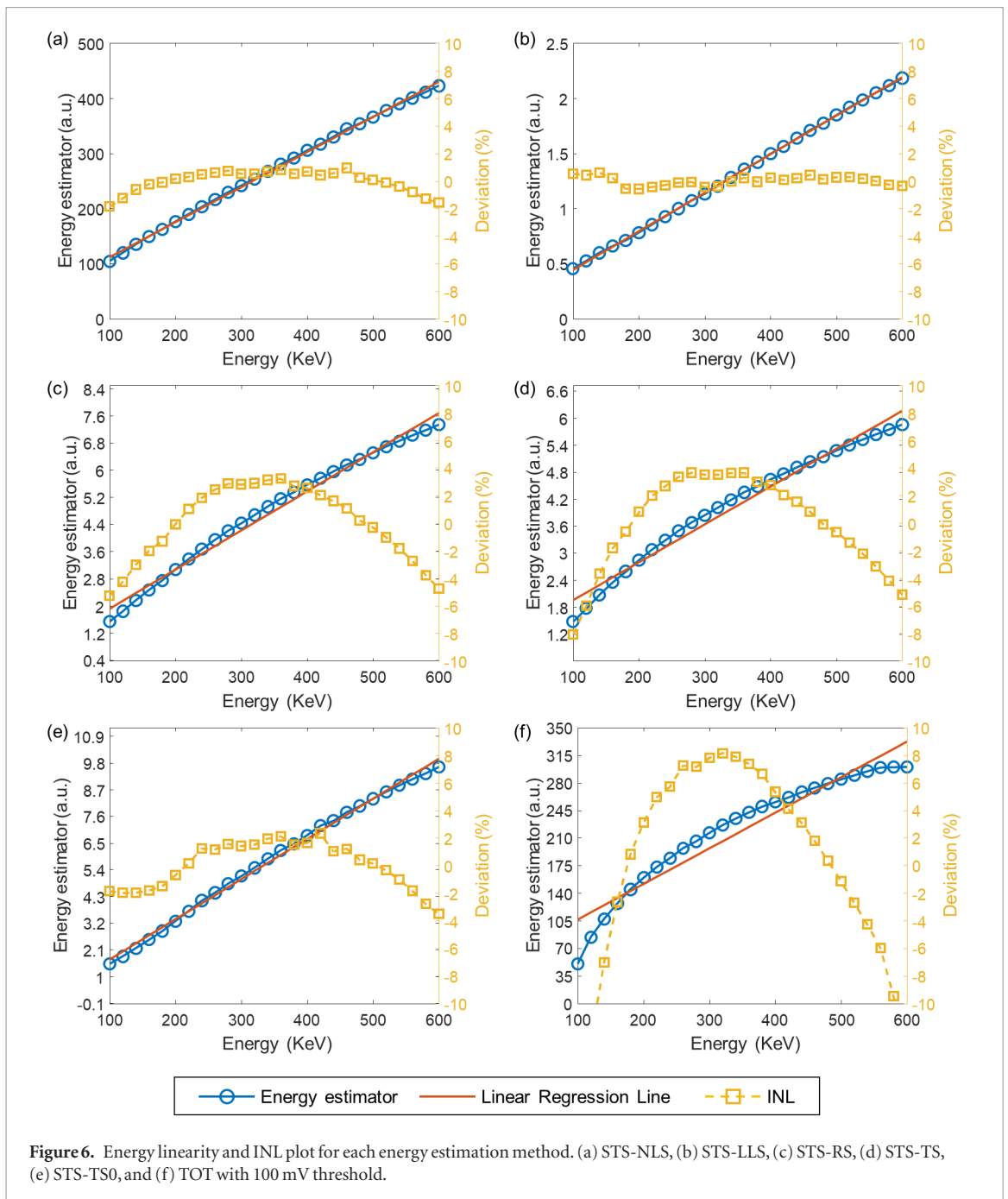


Table 1. Energy estimation performance summary.

Methods	INL _{max} (%)	INL _{min} (%)	INL _{mean} (%)	R ²
STS-NLS	0.945	-1.85	1.34	0.9988
STS-LLS	0.590	-0.594	0.592	0.9998
STS-RS	3.23	-5.28	4.26	0.9872
STS-TS	3.67	-8.09	5.88	0.9764
STS-TS0	2.34	-3.50	2.92	0.9958
TOT (100 mV)	8.15	-22.6	15.4	0.9245

Discussion

In this paper, we have proposed a novel time-based readout method that has several advantages over TOT. Although the proposed STS method is slightly more complex than the simple TOT, it provides better energy and timing performance. STS needs fewer circuit components and digital readout channels than MVT with similar

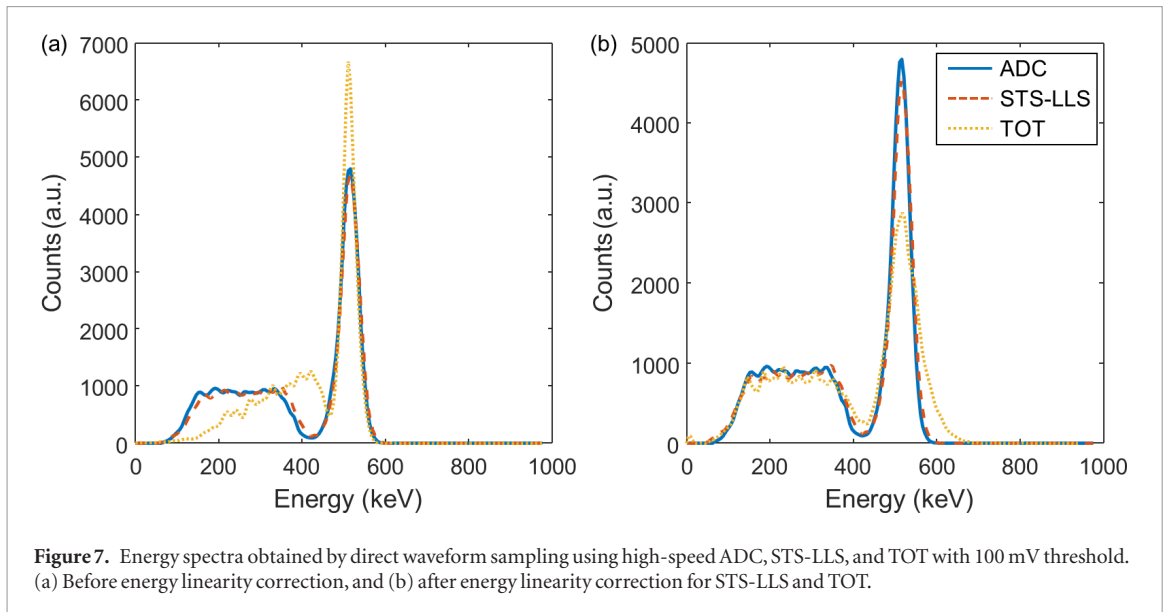


Figure 7. Energy spectra obtained by direct waveform sampling using high-speed ADC, STS-LLS, and TOT with 100 mV threshold. (a) Before energy linearity correction, and (b) after energy linearity correction for STS-LLS and TOT.

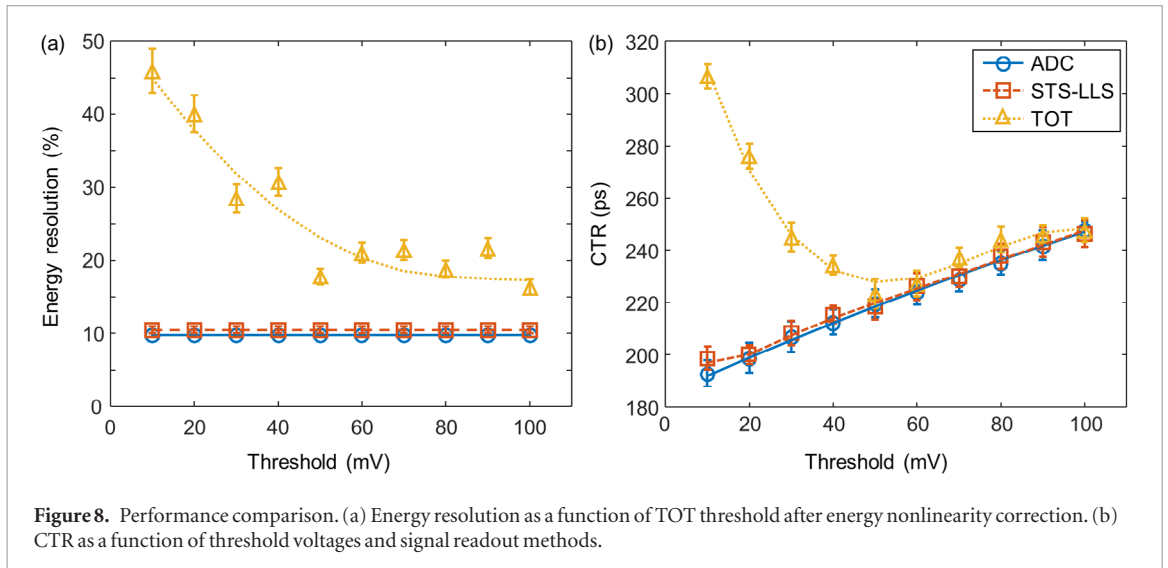


Figure 8. Performance comparison. (a) Energy resolution as a function of TOT threshold after energy nonlinearity correction. (b) CTR as a function of threshold voltages and signal readout methods.

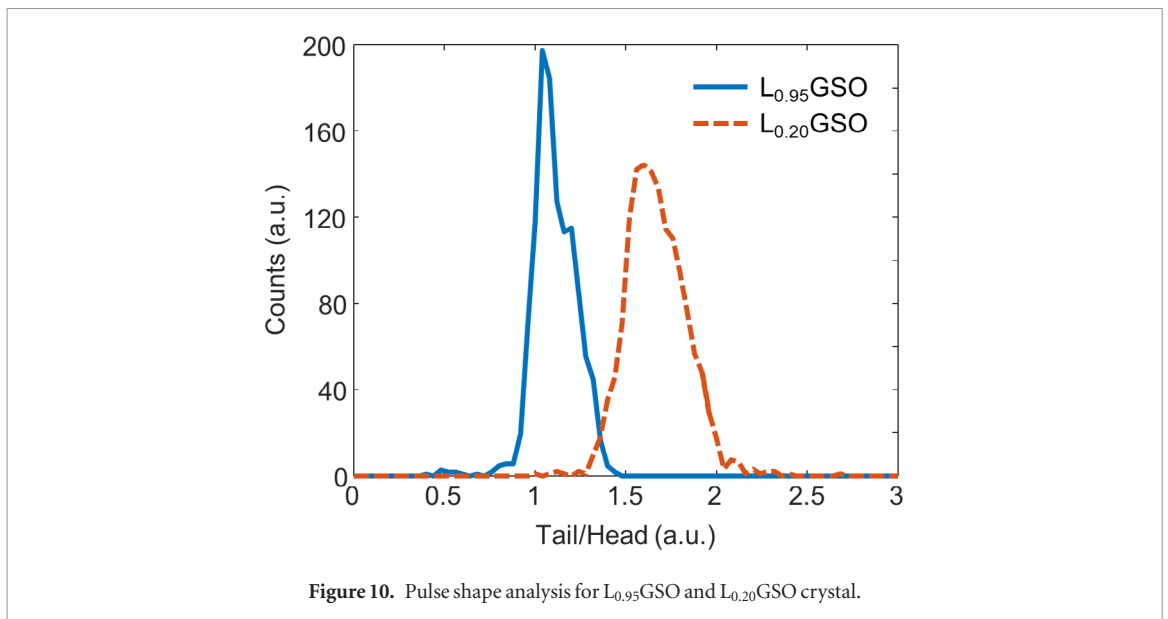
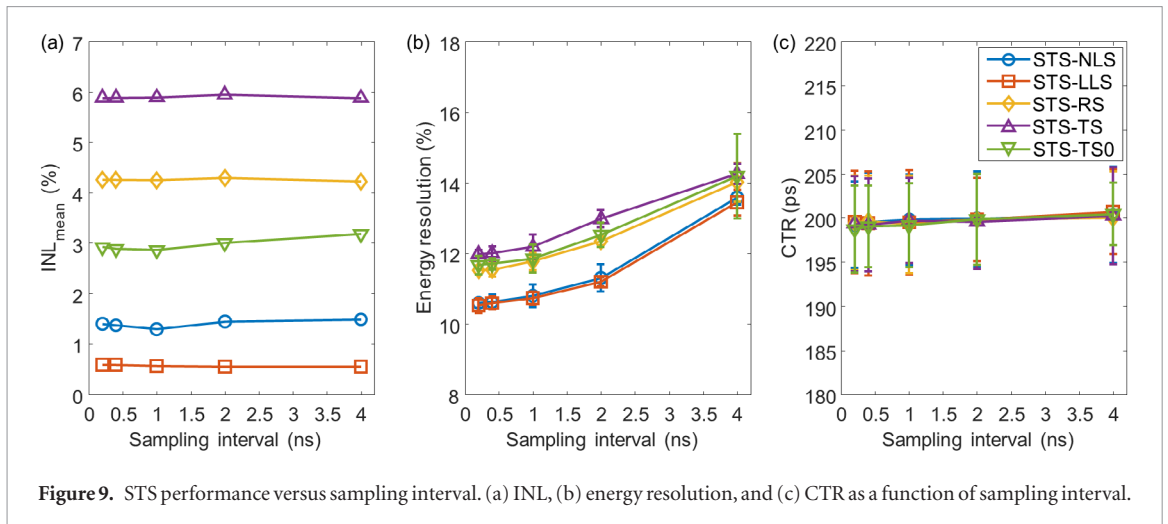
Table 2. Detector performance evaluation summary.

Methods	Energy resolution (%)	CTR (ps) ^a
ADC (5 GHz)	9.84 ± 0.11	193.0 ± 4.3
STS-NLS	10.59 ± 0.14	199.2 ± 4.8
STS-LLS	10.52 ± 0.21	199.6 ± 5.8
STS-RS	11.52 ± 0.13	199.5 ± 5.3
STS-TS	11.97 ± 0.12	199.3 ± 5.4
STS-TS0	11.66 ± 0.26	198.7 ± 4.9
TOT (50 mV)	17.52 ± 0.47	223.5 ± 8.2

^a 10 mV threshold voltage was used for ADC and STS methods.

performance and concept (Xie *et al* 2005). For radiation detection systems with many readout channels, such as PET, the proposed STS method could be efficient for power consumption, cost, and performance.

In the simple TOT method, signal-to-noise ratio of scintillation signal should be sufficiently high to yield good energy resolution. This is because energy is estimated using only two crossing points between scintillation pulse and threshold voltage. Therefore, to improve the energy estimation performance of TOT, a low-pass filter that reduces signal noise should be used. However, low-pass filtering degrades the timing resolution because it blurs the rising edge of the scintillation pulse. On the contrary, STS is more robust to noise because it uses multiple sampling points for energy estimation. Therefore, it can provide good energy performance without low-pass filtering.



In this study, we compared five different energy estimation methods for STS. STS-NLS provides accurate energy information. However, obtaining the NLS solution in real time is difficult because it requires iterative parameter estimation. On the other hand, numerical integration methods (STS-RS, STS-TS, and STS-TS0) have the advantages of lower computation and complexity, which is important in digital logics such as FPGA and DSP. The STS-LLS also has advantages in practical implementation because the solution is obtained through a simple matrix operation. Although it is not discussed in this paper, multiple LLS estimations can be also used for DOI discrimination in PSD as follows: (1) Create a model for the waveform from each scintillation crystal layer. (2) Obtain the LLS solution for all models from the acquired STS signal. (3) Choose the crystal layer that yields smallest least squares error and take the energy of the event.

The cost- and space-effective implementation of STS is possible using a differential input receiver in FPGA as a voltage comparator (Wu *et al* 2007, Xi *et al* 2013). Figure 11 shows the STS circuit implemented using only FPGA and RC filters. In this design, four FPGA input/output (I/O) pins were used to implement an STS device. The tristate buffer on the I/O pin functions as a switch. To avoid false triggers, it is preferred to set the baseline of input signal to less than zero reference voltage of FPGA I/O pin.

Handling many output signal channels without performance degradation is essential for timing resolution in highly accurate PET systems. Our results showed that the difference between the ‘referenced’ CTR with STS readout (199.6 ± 5.8 ps) and the CTR with two identical configuration detectors with high-speed ADC operating at 5 GHz (193.0 ± 4.3 ps) is not quite statistically significant (P value = 0.0752). Therefore, we conclude that the expected CTR with two identical detectors with STS readout is about 200 ps. The STS readout is expected to be an attractive solution for the development of future SiPM-based TOF PET systems.

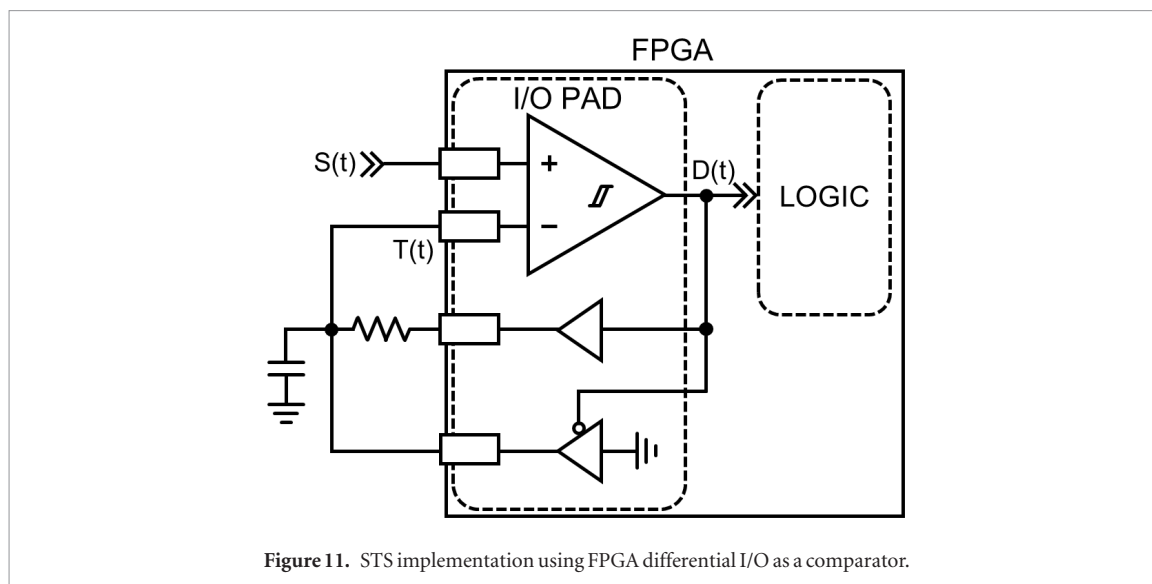


Figure 11. STS implementation using FPGA differential I/O as a comparator.

Conclusion

The proposed readout method reconstructs a scintillation pulse that exponentially decays using only time-based data acquisition. Compared with direct waveform sampling with high-speed ADC, there was almost no degradation in energy and timing resolutions. The proposed method can be a cost-effective solution for data collection in future SiPM-based TOF PET systems.

Acknowledgment

The authors thank Claudio Piemonte and Alessandro Ferri from FBK for the SiPM samples used in this work. This research was supported by Basic Science Research Program through the National Research Foundation of Korea (NRF) funded by the Ministry of Education (NRF-2018R1D1A1B07045559) and Ministry of Science and ICT (NRF-2016R1A2B3014645).

ORCID iDs

Guen Bae Ko  <https://orcid.org/0000-0002-2532-1535>

Jae Sung Lee  <https://orcid.org/0000-0001-7623-053X>

References

- Bergeron M *et al* 2009 Performance evaluation of the LabPET APD-based digital PET scanner *IEEE Trans. Nucl. Sci.* **56** 10–6
- Bieniosek M F, Cates J W, Grant A M and Levin C S 2016 Analog filtering methods improve leading edge timing performance of multiplexed SiPMs *Phys. Med. Biol.* **61** N427–40
- Bieniosek M F, Olcott P D and Levin C S 2013 Compact pulse width modulation circuitry for silicon photomultiplier readout *Phys. Med. Biol.* **58** 5049–59
- Cates J W and Levin C S 2016 Advances in coincidence time resolution for PET *Phys. Med. Biol.* **61** 2255–64
- Chang C-M, Cates J W and Levin C S 2017 Time-over-threshold for pulse shape discrimination in a time-of-flight phoswich PET detector *Phys. Med. Biol.* **62** 258–71
- Conti M 2011 Why is TOF PET reconstruction a more robust method in the presence of inconsistent data? *Phys. Med. Biol.* **56** 155–68
- Dahlbom M, MacDonald L R, Eriksson L, Paulus M, Andreaco M, Casey M E and Moyers C 1997 Performance of a YSO/LSO phoswich detector for use in a PET/SPECT system *IEEE Trans. Nucl. Sci.* **44** 1114–9
- Fu G, Ivan A and Qian H 2016 Recovery of inter-crystal Compton scattering events for sensitivity improvement of sub-250 ps TOF-PET detector 2016 *IEEE Nuclear Science Symp., Medical Imaging Conf. and Room-Temperature Semiconductor Detector Workshop (NSS/MIC/RTSD)* (IEEE) pp 1–5
- Grant A M and Levin C S 2014 A new dual threshold time-over-threshold circuit for fast timing in PET *Phys. Med. Biol.* **59** 3421–30
- Grant A M, Deller T W, Khalighi M M, Maramraju S H, Delso G and Levin C S 2016 NEMA NU 2-2012 performance studies for the SiPM-based TOF-PET component of the GE SIGNA PET/MR system *Med. Phys.* **43** 2334–43
- Hong S J, Kwon S I, Ito M, Lee G S, Sim K-S, Park K S, Rhee J T and Lee J S 2008 Concept verification of three-layer DOI detectors for small animal PET *IEEE Trans. Nucl. Sci.* **55** 912–7
- Ito M, Hong S J and Lee J S 2011 Positron emission tomography (PET) detectors with depth-of-interaction (DOI) capability *Biomed. Eng. Lett.* **1** 70–81
- Kang H G, Ko G B, Rhee J T, Kim K M, Lee J S and Hong S J 2015 A dual-ended readout detector using a meantime method for SiPM TOF-DOI PET *IEEE Trans. Nucl. Sci.* **62** 1935–43

- Karp J S, Surti S, Daube-Witherspoon M E and Muehllehner G 2008 Benefit of time-of-flight in PET: experimental and clinical results *J. Nucl. Med.* **49** 462–70
- Kim H, Kao C M, Xie Q, Chen C T, Zhou L, Tang F, Frisch H, Moses W W and Choong W S 2009 A multi-threshold sampling method for TOF-PET signal processing *Nucl. Instrum. Methods Phys. Res. A* **602** 618–21
- Ko G B and Lee J S 2015 Performance characterization of high quantum efficiency metal package photomultiplier tubes for time-of-flight and high-resolution PET applications *Med. Phys.* **42** 510–20
- Ko G B and Lee J S 2017 Single transmission-line readout method for silicon photomultiplier based time-of-flight and depth-of-interaction PET *Phys. Med. Biol.* **62** 2194–207
- Ko G B, Kim K Y, Yoon H S, Lee M S, Son J W, Im H J and Lee J S 2016a Evaluation of a silicon photomultiplier PET insert for simultaneous PET and MR imaging *Med. Phys.* **43** 72–83
- Ko G B *et al* 2016b Simultaneous multiparametric PET/MRI with silicon photomultiplier PET and ultra-high-field MRI for small-animal imaging *J. Nucl. Med.* **57** 1309–15
- Ko G B, Yoon H S, Kwon S I, Lee C M, Ito M, Hong S J, Lee D S and Lee J S 2013 Development of a front-end analog circuit for multi-channel SiPM readout and performance verification for various PET detector designs *Nucl. Instrum. Methods Phys. Res. A* **703** 38–44
- Kwon S I and Lee J S 2014 Signal encoding method for a time-of-flight PET detector using a silicon photomultiplier array *Nucl. Instrum. Methods Phys. Res. A* **761** 39–45
- Kwon S I, Ferri A, Gola A, Berg E, Piemonte C, Cherry S R and Roncali E 2016 Reaching 200 ps timing resolution in a time-of-flight and depth-of-interaction positron emission tomography detector using phosphor-coated crystals and high-density silicon photomultipliers *J. Med. Imaging* **3** 043501
- Lage E, Parot V, Moore S C, Sitek A, Udias J M, Dave S R, Park M-A, Vaquero J J and Herraiz J L 2015 Recovery and normalization of triple coincidences in PET *Med. Phys.* **42** 1398–410
- Lee J S and Hong S J 2010 Geiger-mode avalanche photodiodes for PET/MRI *Electronic Circuits for Radiation Detection* ed K Iniewski (Boca Raton, FL: CRC Press) pp 179–200
- Lee M S, Kang S K and Lee J S 2018a Novel inter-crystal scattering event identification method for PET detectors *Phys. Med. Biol.* **63** 115015
- Lee S, Lee M S, Kim K Y and Lee J S 2018b Systematic study on factors influencing the performance of interdetector scatter recovery in small-animal PET *Med. Phys.* **45** 3551–62
- Liu C, Wang Y, Kuang P, Li D and Cheng X 2016 A 3.9 ps RMS resolution time-to-digital converter using dual-sampling method on Kintex UltraScale FPGA 2016 *IEEE-NPSS Real Time Conf. (RT)* (IEEE) pp 1–3
- Nemallapudi M V, Gundacker S, Lecoq P, Auffray E, Ferri A, Gola A and Piemonte C 2015 Sub-100 ps coincidence time resolution for positron emission tomography with LSO:Ce codoped with Ca *Phys. Med. Biol.* **60** 4635–49
- Omidvari N, Cabello J, Topping G, Schneider F R, Paul S, Schwaiger M and Ziegler S I 2017 PET performance evaluation of MADPET4: a small animal PET insert for a 7 T MRI scanner *Phys. Med. Biol.* **62** 8671–92
- Park H, Ko G B and Lee J S 2017 Hybrid charge division multiplexing method for silicon photomultiplier based PET detectors *Phys. Med. Biol.* **62** 4390–405
- Parl C, Larue H, Streun M, Ziemons K and van Waasen S 2012 Fast charge to pulse width converter for monolith PET detector *IEEE Trans. Nucl. Sci.* **59** 1809–14
- Piemonte C, Acerbi F, Ferri A, Gola A, Paternoster G, Regazzoni V, Zappala G and Zorzi N 2016 Performance of NUV-HD silicon photomultiplier technology *IEEE Trans. Electron Devices* **63** 1111–6
- Powolny F *et al* 2011 Time-based readout of a silicon photomultiplier (SiPM) for time of flight positron emission tomography (TOF-PET) *IEEE Trans. Nucl. Sci.* **58** 597–604
- Powolny F, Auffray E, Hillemanns H, Jarron P, Lecoq P, Meyer T C and Moraes D 2008 A novel time-based readout scheme for a combined PET-CT detector using APDs *IEEE Trans. Nucl. Sci.* **55** 2465–74
- Schaart D R, Seifert S, Vinke R, Van Dam H T, Dendooven P, Löhner H and Beekman F J 2010 LaBr₃:Ce and SiPMs for time-of-flight PET: achieving 100 ps coincidence resolving time *Phys. Med. Biol.* **55** N179–89
- Schug D *et al* 2016 Initial PET performance evaluation of a preclinical insert for PET/MRI with digital SiPM technology *Phys. Med. Biol.* **61** 2851–78
- Seidel J, Vaquero J J, Siegel S, Gandler W R and Green M V 1999 Depth identification accuracy of a three layer phoswich pet detector module *IEEE Trans. Nucl. Sci.* **46** 485–90
- Shao Y 2007 A new timing model for calculating the intrinsic timing resolution of a scintillator detector *Phys. Med. Biol.* **52** 1103–17
- Shimazoe K, Takahashi H, Boxuan Shi, Orita T, Furumiya T, Ooi J and Kumazawa Y 2012 Dynamic time over threshold method *IEEE Trans. Nucl. Sci.* **59** 3213–7
- Stortz G *et al* 2017 Performance of a PET insert for high resolution small animal PET/MR imaging at 7T *J. Nucl. Med.* **59** 536–42
- Wagadarikar A A, Ivan A, Dolinsky S and McDaniel D L 2014 Sensitivity improvement of time-of-flight (ToF) PET detector through recovery of Compton scattered annihilation photons *IEEE Trans. Nucl. Sci.* **61** 121–5
- Won J Y, Ko G B and Lee J S 2016a Delay grid multiplexing: Simple time-based multiplexing and readout method for silicon photomultipliers *Phys. Med. Biol.* **61** 7113–35
- Won J Y, Kwon S I, Yoon H S, Ko G B, Son J W and Lee J S 2016b Dual-phase tapped-delay-line time-to-digital converter with on-the-fly calibration implemented in 40 nm FPGA *IEEE Trans. Biomed. Circuits Syst.* **10** 231–42
- Wu J, Hansen S and Shi Z 2007 ADC and TDC implemented using FPGA 2007 *IEEE Nuclear Science Symp. Conf. Record* (IEEE) pp 281–6
- Xi D, Kao C-M, Liu W, Zeng C, Liu X and Xie Q 2013 FPGA-Only MVT Digitizer for TOF PET *IEEE Trans. Nucl. Sci.* **60** 3253–61
- Xie Q, Kao C-M, Hsiau Z and Chen C-T 2005 A new approach for pulse processing in positron emission tomography *IEEE Trans. Nucl. Sci.* **52** 988–95
- Yeom J Y, Vinke R and Levin C S 2013 Optimizing timing performance of silicon photomultiplier-based scintillation detectors *Phys. Med. Biol.* **58** 1207–20
- Yin Z, Liu S, Hao X, Gao S and An Q 2012 A high-resolution time-to-digital converter based on multi-phase clock implement in field-programmable-gate-array 2012 *18th IEEE-NPSS Real Time Conf.* (IEEE) pp 1–4
- Yonggang W, Xinyi C, Deng L, Wensong Z and Chong L 2014 A linear time-over-threshold digitizing scheme and its 64-channel DAQ prototype design on FPGA for a continuous crystal PET detector *IEEE Trans. Nucl. Sci.* **61** 99–106
- Yoon H S, Ko G B, Kwon S I, Lee C M, Ito M, Song I C, Lee D S, Hong S J and Lee J S 2012 Initial results of simultaneous PET/MRI experiments with an MRI-compatible silicon photomultiplier PET scanner *J. Nucl. Med.* **53** 608–14